Ultra-long Photoluminescence Lifetime in Inorganic Halide Perovskite Thin Film

Linxing Zhang,[a],* Mei Zhou,[b] Ziyue Zhang,[a] Jifeng Yuan,[a] Bo Li,[a] Wen Wen,[a] Jianjun Tian[a],*

[a] *Institute for Advanced Materials and Technology, University of Science and Technology Beijing, Beijing 100083, China*

[b] *Institute of Applied Physics and Computational Mathematics, Beijing 100088, China*

*E-mail: linxingzhang@ustb.edu.cn, tianjianjun@mater.ustb.edu.cn

Experimental Details

Film fabrication

The etched FTO glasses were cleaned in sequence with deionized water, acetone, and ethanol then further treated under ultraviolet ozone for 10 min. The interlayer of SnO_2 was deposited onto glass/FTO substrates by spin coating at 3000 rpm for 30 s, and then annealed on a hot plate at 150 °C for 30 min. The fixed concentration of SnO_2 colloid precursor was used, which were diluted from the original one ((tin(IV) oxide, H_2O colloidal dispersion, Alfa Aesar). $CsPbI_2Br$ precursor solution at the concentration of 1 M was prepared through dissolving the equimolar PbI_2 (99.9 %, Yingkou, You Xuan Trade Co., Ltd) and CsBr (99.9 %, Aladdin) in the mixed solvents (1:1) of DMF (*N*, *N*-Dimethylformamide, 99.8 %, Sigma-Aldrich) and DMSO (Dimethyl sulfoxide, Sigma-Aldrich) and stirred at 120 °C for 30 min. The $PbBr_2$ (99.99 %, Yingkou, You Xuan Trade Co., Ltd) is used to prepare the other inorganic perovskite systems. Then different weight percentage of PVP (Polyvinyl Pyrrolidone, Vetec™ reagent grade, average mol. wt. 40000) in total weight of CsBr and PbI_2 (Figure S1) have been added to the previous precursor, then aged at least of 24 h. The wet perovskite film was formed by spin-coating the perovskite precursor solution at 5000 rpm for 30 second on glass /FTO/SnO_2. Then the wet transparent film was blew into the semitransparent light brown film by the hot air flow (HAF). Right after that, the film was annealed at different temperature from 180-300 °C for 6 min. All the fabrication steps were performed in the air atmosphere with controlled humidity (~25 °C, 40%<RH<70%). The Ag electrode was deposited by thermal evaporation for photo response measurements.

Characterizations

The crystal structure of the perovskite film was investigated by the X-ray diffraction (XRD), which was performed on the diffractometer (PW3040/60, PANalytical, Holland) with Cu Kα radiation. The morphologies were determined by the scanning electron microscopy (SEM) measurement, which was performed using a cold field

emission scanning electron microscope (SU4800, Hitachi). The absorption spectra were collected using an ultraviolet-visible (UV-vis) spectrophotometer (T10, Persee). Steady-state photoluminescence (PL) measurement were measured using a fluorescence spectrophotometer with a xenon lamp coupled to a monochromator (F-380, Gangdong) with a 400 nm of excitation wavelength. PL quantum efficiency (PLQE) measurements were acquired using an integrating sphere setup (FLS980, Edinburg) with a 470 nm of excitation wavelength. The photoluminescence (PL) decay spectra were measured using a time-resolved fluorescence spectrometer (FLS900, Edinburg), and the excitation wavelength was 450 nm. The confocal PL maps were acquired using a single-photon counting confocal microscope (LSM Upgrade, PicoQuant). Fourier transform infrared (IR) spectra (KBr pellet) were recorded using Varian-3100FTIR spectrometer. The photocurrent density-voltage (I-V) characteristics were measured using the digital source meter (2400, Keithley Instruments Inc.) under AM 1.5 G illumination simulated sunlight (100 mW cm^{-2}) (7-SS1503A, 7 Star Optical Instruments Co., Beijing, China).

Calculation methods

The first-principle calculations were performed in the framework of density functional theory (DFT)[39,40] using the Vienna ab-initio Simulation Package (VASP).[41-43] The Perdew-Burke Ernzerhof (PBE)[44] exchange correlation function with the projected augmented wave (PAW)[45,46] method was used for geometry optimization and calculations of the total energy. The wave functions of the valence electrons were calculated using a plane wave basis set with 400 eV cutoff energy. The van der Waals interaction (vdW)[47] was included using DFT-D3 method to accurately relax the atomic structure.[48] We simulate the halide (001) (terminated by Cs/Pb) surfaces by periodic p(2×1) and p($\sqrt{2} \times \sqrt{2}$) slabs consisting of 6 atomic layers with the vacuum space between neighbors of about 20 Å to avoid artificial interactions, respectively. Throughout the simulations, bottom three atomic layers are kept frozen whereas all the remaining atoms are free to relax. In the atomic structural relaxations and total energy

calculations, the Monkhorst-Pack mesh with $3 \times 5 \times 1$ and $5 \times 5 \times 1$ K-points were used to integral the reciprocal space for halide (001) (terminated by Cs/Pb) surfaces. The adsorption energies of PVP-halide (001) (terminated by Cs/Pb) surfaces are calculated using the expression below:

$$E_{ad} = E_{PVP\_slab} - \left(E_{slab} + E_{PVP}\right)$$

Where E_{slab}, E_{PVP} and E_{PVP_slab} are the total energy of the relaxed clean slab, the isolated PVP and the slab covered with PVPs. According to this definition, the larger adsorption energy, the stronger interaction between PVP and the substrate.

The position of I and Br really should be significant to the results of DFT. It is very difficult to consider the random arrangement of I and Br, so we chose an ordered substitution in the calculation. We consider two replacement positions of Pb-I octahedron in CPI2, namely, the out-of-plane direction (CPI2-1) and the in-plane direction (CPI2-2), as shown in the followed Figure. The Br replacement position of out of plane (CPI2-1) is the purple dotted circle. The Br replacement position of in plane (CPI2-2) is the green dotted circle. As shown in the Table S2, exactly, the absorption energy is different for CPI2-1, CPI2-2 and CPI3. However, all O-Pb energy show the highest one. The C1-Pb of CPI2-2 cannot be converged, so we didn't get the corresponding value. In the main manuscript, the data is the one of the out-of-plane direction.
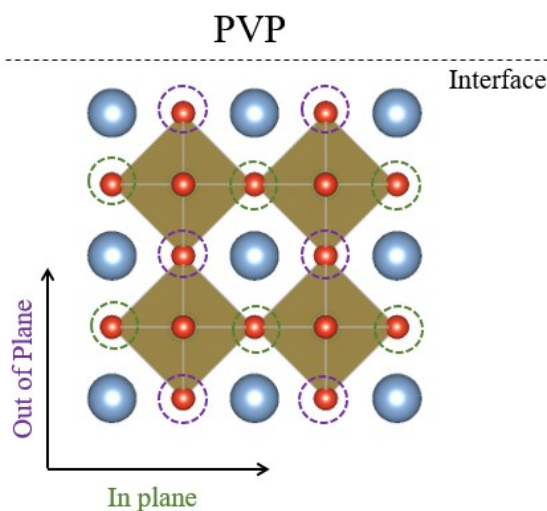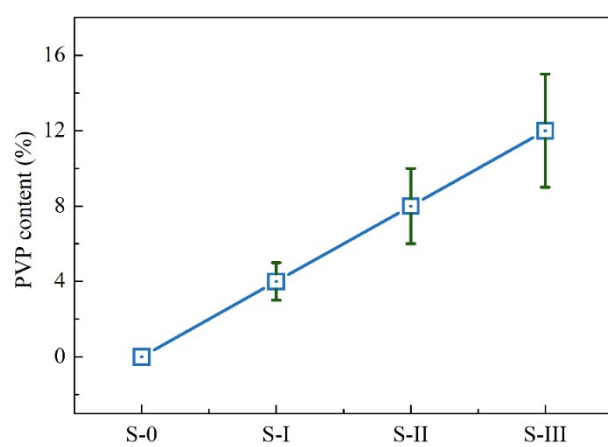
Figure S1 PVP content of S-0, S-I, S-II, and S-III in CPI2 inorganic thin films, which is designed during the experiment process.
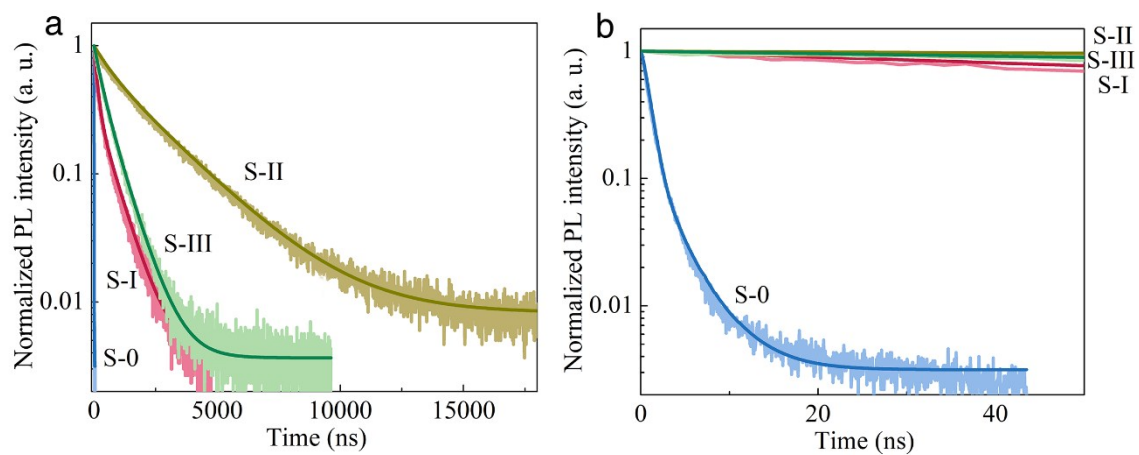
Figure S2 (a) Wide range and (b) narrow range of time-resolved PL decay measurement of CPI2 inorganic perovskite of S-0, S-I, S-II, and S-III, respectively.
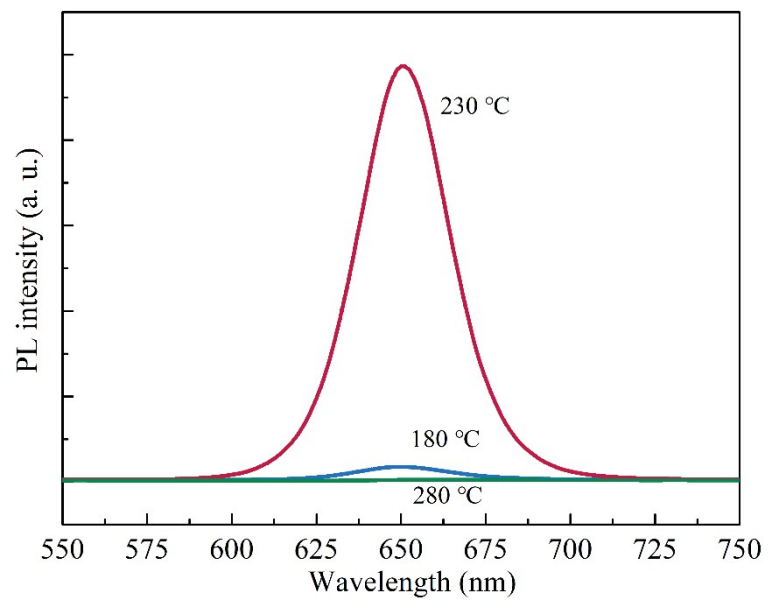
Figure S3 Steady-state PL measurement in the S-II films of CPI2 with different annealing temperature.

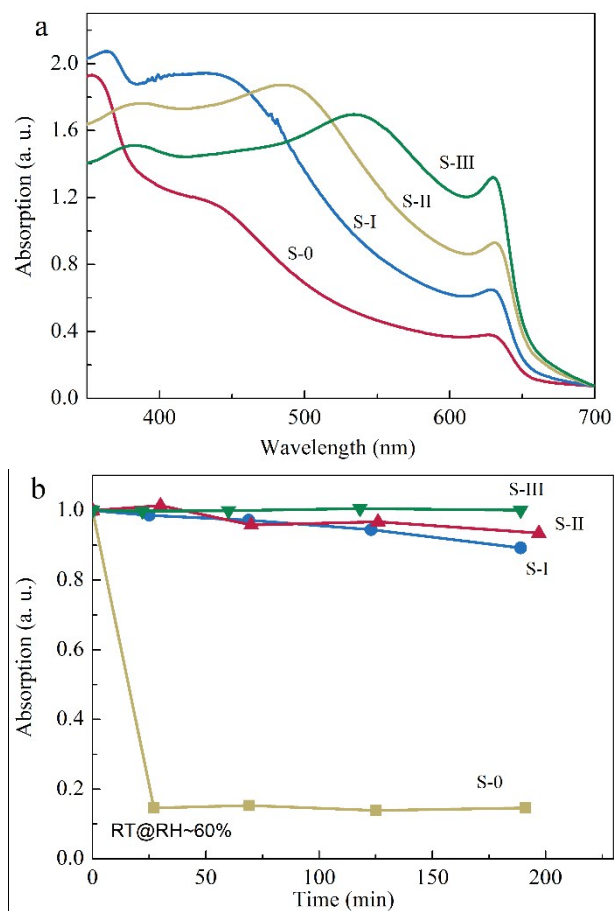**Figure S4** (a)The UV-Vis absorption spectra of S-0, S-I, S-II and S-III. The bulge peaks of S-I, S-II and S-III between wavelength of 400 nm and 600 nm would be ascribed to the discontinuous grains of the films. (b) The stability of the present inorganic CPI2 films with PVP passivation at the air atmosphere with high humidity of ~60%. The absorption value extracted at wavelength of 450 nm in absorption spectra.
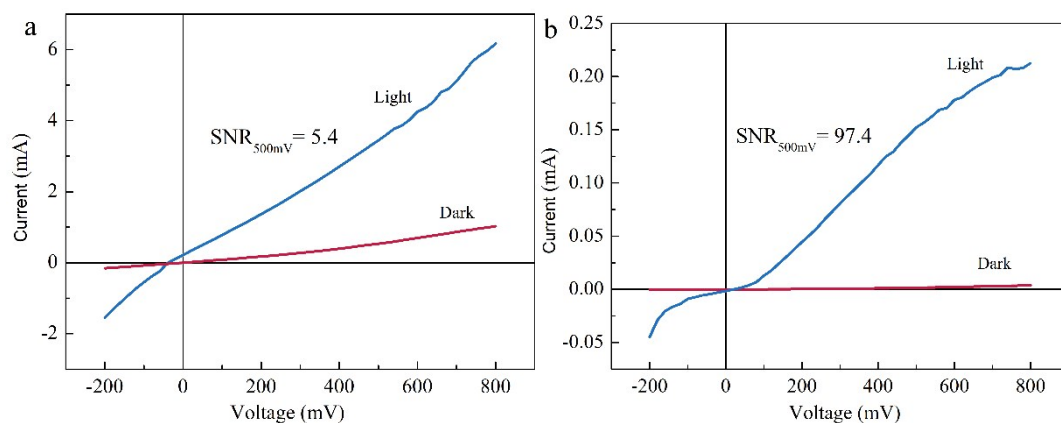
Figure S5 *I-V* curve under light and dark of present inorganic perovskite devices (a) without PVP passivation (S-0) and (b) with PVP passivation (S-II). Both of S-0 and S-II possess the photo response under light. Although the current value of S-0 is an order of magnitude larger than that of S-II, we find that the signal-to-noise ratio (SNR defined as $(I_{light}-I_{dark})/I_{dark}$ ratio) of S-II (~97.4) is 18 times larger than that of S-0 (~5.4). This indicates that the passivation of PVP should show outstanding photosensitive characteristics for optoelectronic performance.

Table S1 The PL lifetimes of the present CPI2 films and the other reporting systems of semiconductor materials from references.

System	Lifetime (ns)	Reference
CsPbBr$_3$ (CPI0)		
CPI0/TiO$_2$/FTO	116.2	15
CPI0/ZnO/FTO	2.1	16
CPI0/SnO$_2$/FTO	1.2	This work
CPI0-PVP/SnO$_2$/FTO	6.1	This work
CsPbIBr$_2$ (CPI1)		
CPI1/TiO$_2$/FTO	17.5	19
CPI1/Glass	3.2	20
CPI1/SnO$_2$/FTO	0.8	This work
CPI1-PVP/SnO$_2$/FTO	25.3	This work
CsPbI$_2$Br (CPI2)		
CPI2/Al$_2$O$_3$/Glass	11.1	21
CPI2-Sr/Al$_2$O$_3$/Glass	17.1	21
CPI2/Glass	14	22
CPI2-K/Glass	11	22
CPI2/TiO$_2$/FTO	4.0	9
CPI2/Glass	14	23
CPI2/TiO$_2$/FTO	35.5	24
CPI2-Ge/FTO	13.1	25
CPI2/TiO$_2$/ITO	6.9	26
CPI2-P3HT/TiO$_2$/ITO	14.8	26
CPI2/SnO$_2$/FTO	1.3	This work
CPI2-PVP/SnO$_2$/FTO	2530.5	This work
CsPbI$_3$ (CPI3)		
CPI3-SCG/SnO$_2$/ITO	5.2	27
CPI3-QD/Glass	1.8	17
CPI3/Glass	19.3	18
CPI3-PVP/Glass	338.7	18
CPI3/SnO$_2$/FTO	5.5	This work
CPI3-PVP/SnO$_2$/FTO	12.4	This work
MAPbI$_3$ (MPI3)		
MPI3/Glass	340.7	11
MPI3-Pyridine/Glass	2234.2	11
MPI3/Glass	736	12

MPI3-TOPO//Glass	8820	13
Other Semiconductors		
GaAs	1000	14
Si	>10000	14

Table S2 Absorption energy (kJ/mol) of different groups-CPI2 (or CPI3) films, which are the calculation results.

	CPI2-1	CPI2-2	CPI3
C2-Pb	17.62	72.99	0.22
C1-Pb	-9.57	-	-27.73
O-Pb	**45.28**	**95.76**	**39.75**
C2-Cs	-19.04	-32.07	-14.92
C1-Cs	-31.00	-22.03	-51.09
O-Cs	**14.64**	**15.77**	**5.22**

Table S3 The FWHM of (002) peaks in XRD for two series samples of S-0, S-I, S-II, and S-III films, respectively.

	First series samples		Second series samples	
	PVP content	FWHM (°)	PVP content	FWHM (°)
S-0	0 %	0.19	0 %	0.17
S-I	5 %	0.25	3%	0.19
S-II	10 %	0.15	6%	0.18
S-III	15 %	0.14	9%	0.16

Table S4 The location, FWHM, Intensity, and ratio of steady-state PL measurement of CPI2 inorganic perovskite of S-0, S-I, S-II, and S-III films, respectively.

	Location (nm)	FWHM (nm)	Intensity (a. u.)	Ratio
S-0	651.2	34	26	-
S-I	650.9	30	69	2.7
S-II	648.6	30	1638	63
S-III	649.5	31	460	17.7

Table S5 The detailed parameters of time-resolved PL decay measurement of CPI2 inorganic perovskite of S-0, S-I, S-II, and S-III, respectively. They are fitted with a bi-exponential decay model. The PL lifetime is considered as the summation of fast- and slow-decay components that give a short lifetime τ_1 and a long lifetime τ_2, respectively. The fraction for τ_1 and τ_2 are A_1 and A_2, respectively. The average carrier lifetimes can be calculated by the formula of $<\tau> =(A_{1*}\tau_{1+} A_{2*}\tau_2)/100$.

	S-0	S-I	S-II (1)	S-II (2)	S-II (3)	S-III
A_1 (%)	84.4	27.6	9.9	10.8	12.7	26.0
τ_1 (ns)	0.8	132.3	660.9	352.8	609.5	306.0
A_2 (%)	15.6	72.4	90.1	89.2	87.3	74.0
τ_2 (ns)	3.7	666.0	2343.2	2793.6	2192.4	701.6
$<\tau>$ (ns)	1.3	518.7	2176.4	2530.5	1991.4	598.6

References

39 P. Hohenberg and W. Kohn, *Phys. Rev.*, 1964, **136**, B864.

40 W. Kohn and L. J. Sham, *Phys. Rev.*, 1965, **140**, A1113.

41 G. Kresse and J. Hafner, *Phys. Rev.*, B 1994**, 49**, 251.

42 G. Kresse and J. Furthmuller, *Comput. Mater. Sci.*, 1996, **6**, 15.

43 G. Kresse and J. Furthmuller, *Phys. Rev. B*, 1996, **54**, 11169.

44 J. P. Perdew, K. Burke and M. Ernzerhof, *Phys. Rev. Lett.*, 1996, **77**, 3865.

45 P. E. Blchl, *Phys. Rev. B*, 1994, **50**, 17953.

46 G. Kresse and D. Joubert, *Phys. Rev. B*, 1999, **59**, 1758.

47 Y. Ding, M. Iannuzzi and J. Hutter, *J. Phys. Chem. C*, 2011, **115**, 13685.

48 S. Grimme, J. Antony, S. Ehrlich and S. Krieg, *J. Chem. Phys.*, 2010, **132**, 154104.